Double photoionization of beryllium

J. Colgan and M. S. Pindzola
Department of Physics, Auburn University, Auburn, Alabama 36849
(Received 18 June 2001; published 15 January 2002)

The time-dependent close-coupling method is used to obtain absolute results for total integral, single energy, and angle differential cross sections for the double photoionization of beryllium. We compare the total ionization cross section to previous perturbative and recent nonperturbative calculations. We also compare and contrast the triple differential cross sections obtained at 20 eV excess photon energy with those obtained recently for helium [J. Phys. B **34**, L457 (2001)].

DOI: 10.1103/PhysRevA.65.022709 PACS number(s): 32.80.Fb

I. INTRODUCTION

It is well known that direct double photoionization studies provide the simplest method for exploring correlation effects in the two-electron continuum. In particular, angular electron distributions provide the most sensitive test of correlation and so have been the subject of intensive work, both theoretically and experimentally, in recent years.

Most recent studies have concentrated on the simplest two-electron system, the helium atom. Much experimental work has been done [1–3] yielding double-to-single photoionization ratios; also absolute triple differential cross-section measurements have been made [4–6] using recoil ion momentum spectroscopy techniques. On the theoretical side, integral and differential cross sections have been calculated using various nonperturbative methods including the double-screened Coulomb [7,8], convergent close coupling [9,10], the hyperspherical R matrix [11,12], and the time-dependent close coupling [13,14]. The most recent of each of these types of calculations of triple differential cross sections are in excellent agreement with experiment.

In this paper, we extend our time-dependent close-coupling method to the study of double photoionization processes in the beryllium atom. Although we are aware of no experimental measurements for Be, and only several perturbative theoretical calculations of the total double photoionization cross section [15,16], these calculations mark the start of a systematic study of absolute total and differential cross sections for the alkaline-earth metals. Very recently, there have been nonperturbative calculations of total integral cross sections for beryllium using the convergent close-coupling method [17]. We compare wherever possible with these ongoing calculations and find excellent agreement. There has been some recent experimental measurements of triple differential cross sections in calcium [18–20] as well as several theoretical studies [21,22] of the alkaline earth metals. However, only relative differential cross sections were measured or calculated. This paper contains absolute calculations for triple differential cross sections of an alkaline-earth element. The rest of this paper is structured as follows. In Sec. II, we describe the time-dependent close-coupling method as applied to double photoionization calculations. In Sec. III, we present results for total, energy differential, and angular differential cross sections of Be. Finally, in Sec. IV, we give a short summary.

II. METHOD

The time-dependent close-coupling theory has been well described in previous double photoionization studies of helium [13,14]. Here, we describe the extension of the theory to include double photoionization of the alkaline-earth metals.

A. Use of a pseudopotential

The $1s^2$ ground state of Be^{2+} is calculated in the Hartree-Fock approximation. A set of bound $\overline{nl}$ and continuum $\overline{kl}$ radial orbitals is then obtained by diagonalization of the one-dimensional Hamiltonian given by

$$h(r) = -\frac{1}{2}\frac{\partial^2}{\partial r^2} + \frac{l(l+1)}{2r^2} - \frac{Z}{r} + V_D(r) + V_X(r), \qquad (1)$$

where $V_D(r)$ and $V_X(r)$ are the direct Hartree and local exchange potentials, respectively, $Z=4$ is the nuclear charge of the target, and atomic units are used throughout. The potentials are calculated using the $1s$ orbital and a parameter in the exchange term is adjusted so that the single-particle energies for each angular momentum are in good agreement with the configuration-average experimental spectrum [23]. The inner node of the $2s$ wave function is eliminated and a pseudopotential is then found that generates the nodeless $2s$ orbital. Subsequently, all the $\overline{ns}$ and $\overline{ks}$ bound and continuum orbitals are generated using this pseudo-potential. The $\overline{2s}$ pseudo-orbital is very similar to the $2s$ orbital found from a Hartree-Fock calculation for the ground state of Be^+. We note that, for a fixed box size, the energy distribution of bound and continuum states changes for each angular momentum.

We may also obtain the continuum state radial orbitals by direct numerical integration of the time-independent Schrödinger equation for Be^+

$$\left(h(r) - \frac{k^2}{2}\right) P_{kl}(r) = 0. \qquad (2)$$

We choose the standard box normalization given by

 ©2002 The American Physical Society

$$P_{kl}(r) \rightarrow \sqrt{\frac{2\Delta k}{\pi}} \sin\left(kr + \frac{q}{k} \ln(2kr) - \frac{l\pi}{2} + \sigma_l + \delta_l \right), \tag{3}$$

where Δk is the momentum mesh spacing, $q=2$ is the asymptotic charge, σ_l is the Coulomb phase shift, and δ_l is the distorted-wave phase shift. Note that as the density of states increases for smaller Δk mesh spacing, the amplitude of any one continuum wave decreases. We use a total of 600 continuum state radial orbitals on a uniform momentum mesh with $\Delta k = 0.0025$. In generating the continuum functions by this direct numerical integration over a fixed momentum mesh, with the box normalization as defined, we ensure that, for all angular momenta, the continuum-orbital amplitudes are calculated at the same energy points. This allows us to add the continuum-orbital amplitudes coherently, which is necessary in the calculation of the angle differential cross sections. We remark also that we have calculated the total double photoionization and single differential cross section using both methods of generating continuum orbitals and found excellent agreement between the two methods.

B. Partial correlation of the ground state

The ground state of beryllium is found by relaxation of the time-dependent Schrödinger equation in imaginary time ($\tau = it$)

$$-\frac{\partial \Phi_0^{1S}(\vec{r}_1, \vec{r}_2, \tau)}{\partial \tau} = H_{\text{atom}} \Phi_0^{1S}(\vec{r}_1, \vec{r}_2, \tau), \tag{4}$$

where the nonrelativistic Hamiltonian is given by

$$H_{\text{atom}} = -\frac{1}{2}\nabla_1^2 - \frac{1}{2}\nabla_2^2 + V_{pp}(r_1) + V_{pp}(r_2), \tag{5}$$

where, for $l>0$, the pseudopotentials are given by $V_{pp}(r) = -Z/r + V_D(r) + V_X(r)$. The six-dimensional ground-state wave function is expanded in coupled spherical harmonics

$$\Phi_0^{1S}(\vec{r}_1, \vec{r}_2, \tau) = \sum_{l=0}^{l_0} \frac{P_{ll}^{1S}(r_1, r_2, \tau)}{r_1 r_2} Y_{ll}^{1S}(\hat{r}_1, \hat{r}_2), \tag{6}$$

where it was found that up to $l_0 = 6$ is required for convergence of all angular differential cross sections. Substituting Eqs. (6) and (5) into Eq. (4) yields a set of coupled partial differential equations for the two-dimensional radial wave functions $P_{ll}^{1S}(r_1, r_2, \tau)$ that may be solved on a numerical lattice using standard finite difference methods [13]. About 1000 imaginary time steps at $\Delta\tau = 0.005$ are needed to achieve convergence on a uniform lattice with a mesh spacing of $\Delta r = 0.1$ if one begins with $P_{ll}^{1S}(r_1, r_2, \tau=0) = \delta_{l,0} P_{2s}^{-}(r_1) P_{2s}^{-}(r_2)$, where $P_{2s}^{-}(r)$ is a bound-state radial orbital for Be^+.

It is important to state here that the beryllium ground-state wave function is correlated, in that the $2s^2$ orbital is a superposition of $(s^2 + p^2 + d^2 + \cdots)$ wave functions. The introduction of a pseudopotential has restricted any inclusion of orbitals containing promotions from the $1s^2$ core, which will place a limit on the accuracy that can be achieved in the calculation of the total energy of the beryllium ground state. However, in considering two-electron photoionization in an energy range well below the $1s^2$ threshold, it is unlikely that the $1s^2$ orbital will come into play, and so our use of a pseudopotential is justified. We note also that this correlated ground-state wave function for beryllium has a total energy that is within 1% of the experimental total energy [24].

C. Length gauge versus velocity gauge

We now solve the ''weak field'' time-dependent Schrödinger equation in real time

$$i\frac{\partial \Psi^{1P}(\vec{r}_1, \vec{r}_2, t)}{\partial t} = H_{\text{atom}} \Psi^{1P}(\vec{r}_1, \vec{r}_2, t) + H_{\text{rad}} \Phi_0^{1S} \times (\vec{r}_1, \vec{r}_2, \tau=\infty) e^{-iE_0 t}, \tag{7}$$

where the Hamiltonian for a linearly polarized radiation field in the length gauge is given by

$$H_{\text{rad}} = E(t)(r_1 \cos\theta_1 + r_2 \cos\theta_2)\cos\omega t, \tag{8}$$

with electric-field amplitude $E(t)$ and radiation frequency ω.

In previous calculations of double ionization processes in helium, it was found that our results were almost completely invariant under use of either the length or velocity gauges, for all cross sections calculated. In this case, our use of a pseudopotential complicates matters. By removing the inner node of the $2s$ radial wave function, we have invalidated the use of the velocity gauge, which emphasizes the inner region of the wave function. As an illustration on the use of the velocity gauge with our radial orbitals generated using the pseudopotential, the radiative rate for the $1s^2 2s^2\ {}^1S \rightarrow 1s^2 2s 2p\ {}^1P$ transition in Be was calculated, in both length and velocity gauges, using both orbitals calculated in a Hartree-Fock potential and orbitals calculated in the pseudopotential.

In the Hartree-Fock potential, the transition rate was found to be 5.41×10^8 and 2.62×10^8 Hz in the length and velocity gauges, respectively. The difference between these two calculations is due to the nonlocal Hartree-Fock operator, but is sufficient for our purposes here. Using the pseudopotential, the transition rate was found to be 5.51×10^8 and 7.48×10^8 Hz in the length and velocity gauges, respectively. It is clear that, while in the length gauge the transition rate has changed only slightly using the modified orbitals, in the velocity gauge, the transition rate has changed by a factor of four. This simple test confirms that use of a pseudopotential under the velocity gauge is unreliable. We note also that the length gauge calculation agrees well with the experimental value of 5.56×10^8 Hz [23]. Therefore, we present here only results calculated in the length gauge.

D. Definition of total and angular differential cross sections

The six-dimensional photoabsorption state wave function is also expanded in coupled spherical harmonics

$$\Psi^{^1P}(\vec{r}_1,\vec{r}_2,t)=\sum_{l_1,l_2}\frac{P^{^1P}_{l_1l_2}(r_1,r_2,t)}{r_1r_2}Y^{^1P}_{l_1l_2}(\hat{r}_1,\hat{r}_2), \quad (9)$$

where $l_1 \leqslant 6$ and $l_2 \leqslant 6$ is sufficient. Substituting Eqs. (5), (6), (8), and (9) into Eq. (7) yields a set of coupled partial differential equations for the two-dimensional radial wave functions, $P^{^1P}_{l_1l_2}(r_1,r_2,t)$, that may also be solved on a numerical lattice [13]. Keeping the same mesh spacing of $\Delta r = 0.1$ and beginning with $P^{^1P}_{l_1l_2}(r_1,r_2,t=0)=0$ for all l_1,l_2, the close-coupled equations are time propagated for up to 10 radiation field periods $(2\pi/\omega)$. A lattice size of 600×600 points is employed. Increasing the lattice to 1000×1000 points made a difference of no more than 2% in the results presented here.

The total photoabsorption probability is given by

$$\mathcal{P}=\sum_{l_1,l_2}\int_0^\infty dr_1\int_0^\infty dr_2|P^{^1P}_{l_1l_2}(r_1,r_2,t)|^2. \quad (10)$$

Using standard projection techniques, the total double photoionization probability is given by

$$\mathcal{P}_{\rm dion}=\sum_{l_1,l_2}\int_0^\infty dk_1\int_0^\infty dk_2|P^{^1P}_{l_1l_2}(k_1,k_2,t)|^2, \quad (11)$$

where

$$P^{^1P}_{l_1l_2}(k_1,k_2,t)=\int_0^\infty dr_1\int_0^\infty dr_1P_{k_1l_1}(r_1)\times P_{k_2l_2}(r_2)P^{^1P}_{l_1l_2}(r_1,r_2,t), \quad (12)$$

and $P_{kl}(r)$ is a continuum state radial orbital for Be^+, which is obtained by the diagonalization of Eq. (1) or by integrating Eq. (2). Both total probabilities may be monitored as a function of time. Time propagations have converged when the rate of change of the total double photoionization probability becomes constant. In general, larger lattice sizes and longer propagation times are needed as the excess photon energy, defined by $\Delta E=\omega+E_0$, becomes smaller.

The total integral cross section for double photoionization is given by

$$\sigma_{\rm dion}=\frac{\omega}{I}\frac{\partial\mathcal{P}_{\rm dion}}{\partial t}, \quad (13)$$

where I is the radiation field intensity.

The single differential cross section for double photoionization may be defined as

$$\sigma_{\rm dion}=\int_0^{\pi/2}\frac{d\sigma}{d\alpha}d\alpha=\int_0^{\Delta E}\frac{d\sigma}{dE_1}dE_1, \quad (14)$$

where $E_1=k_1^2/2$. The hyperspherical angle differential cross section is given by

$$\frac{d\sigma}{d\alpha}=\frac{\omega}{I}\frac{\partial}{\partial t}\int_0^\infty dk_1\int_0^\infty dk_2\delta\left[\alpha-\tan^{-1}\left(\frac{k_2}{k_1}\right)\right]\times\sum_{l_1,l_2}|P^{^1P}_{l_1l_2}(k_1,k_2,t)|^2. \quad (15)$$

The ejected-energy differential cross section is then defined as

$$\frac{d\sigma}{dE_1}=\frac{1}{k_1k_2}\frac{d\sigma}{d\alpha}, \quad (16)$$

where the transformation factors in the denominator will make the ejected-energy differential cross section less peaked along the $k_1=k_2$ axis than the hyperspherical angle differential cross section.

The triple differential cross section for double photoionization can be written as

$$\sigma_{\rm dion}=\int_0^{\pi/2}d\alpha\int d\Omega_1\int d\Omega_2\frac{d^3\sigma}{d\alpha d\Omega_1 d\Omega_2}. \quad (17)$$

Since for long times following the collision $\vec{r}\rightarrow\vec{k}T$, the differential cross section in hyperspherical angle and the solid angles for the emission of both photoelectrons is given by

$$\frac{d^3\sigma}{d\alpha d\Omega_1 d\Omega_2}=\frac{\omega}{I}\frac{\partial}{\partial t}\int_0^\infty dk_1\int_0^\infty dk_2\delta\left[\alpha-\tan^{-1}\left(\frac{k_2}{k_1}\right)\right]\times\left|\sum_{l_1,l_2}(-i)^{l_1+l_2}e^{i(\delta_{l_1}+\delta_{l_2})}e^{i(\sigma_{l_1}+\sigma_{l_2})}\times P^{^1P}_{l_1l_2}(k_1,k_2,t)Y^{^1P}_{l_1l_2}(\hat{k}_1,\hat{k}_2)\right|^2. \quad (18)$$

In contrast to Eq. (15), the sum over l_1l_2 is now inside the square so that the outgoing momentum space wave-function amplitudes are summed coherently. Since we make use of a projection in Eq. (12) onto products of distorted waves, the momentum space amplitudes must be weighted by their distorted (denoted by δ_l) and Coulomb (denoted by σ_l) phase shifts. We note that in this case, for $l>0$, the wave functions have a positive phase shift, but for $l=0$, the wave function is shifted inwards due to the node removal by the pseudopotential. Care must be taken to ensure the correct phase shifts are used, as this is critical in the determination of triple differential cross sections. Finally, the orthonormality relations for the coupled momentum spherical harmonics guarantee reduction of Eq. (18) to Eq. (15) upon integration over the solid angles for both photoelectrons.

III. RESULTS

Total double photoionization cross sections at various excess photon energies calculated using the time-dependent close-coupling method are presented in Fig. 1 along with two other perturbative theoretical calculations [15,16], and a non-

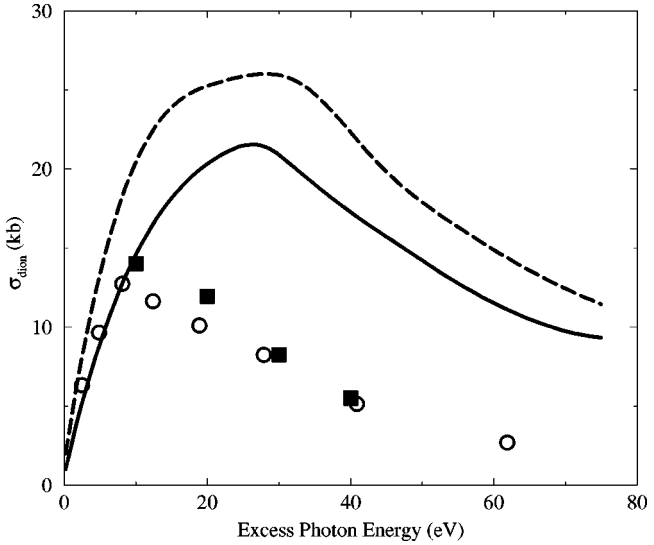

FIG. 1. Total double photoionization rate for beryllium. The solid squares are the current time-dependent close-coupling calculations, the open circles are the convergent close-coupling calculations of [17], the solid line is the result estimated from Winkler [15], and the dashed line is the result estimated from Varnavskikh [16]. (1.0 kb$=1.0\times10^{-21}$ cm^2.)

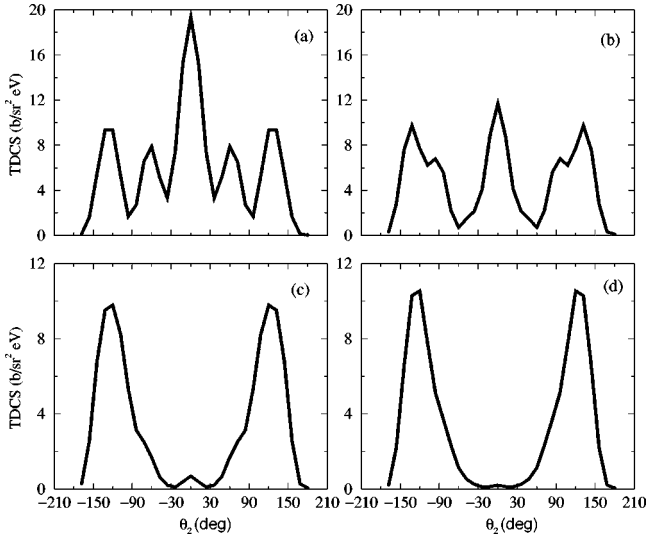

FIG. 3. Triple differential cross section in b/sr^2 eV for beryllium at 20 eV excess photon energy and at equal energy sharing between the two outgoing electrons as a function of θ_2, the angle of the second ejected electron for $\theta_1=0$. The cross sections are calculated with (a) $l_0\leqslant3,l_1,l_2\leqslant3$, (b) $l_0\leqslant4,l_1,l_2\leqslant4$, (c) $l_0\leqslant5,l_1,l_2\leqslant5$, and (d) $l_0\leqslant6,l_1,l_2\leqslant6$, respectively, in Eqs. (6) and (9). (1.0 b$=1.0\times10^{-24}$ cm^2.)

perturbative convergent close-coupling calculation [17]. We find that the nonperturbative time-dependent calculations are up to 50% lower than the previous perturbative calculations, and in excellent agreement with the convergent close-coupling calculations at a range of excess photon energies, and that the peak of the cross section is much closer to threshold than suggested by the perturbative calculations. Unfortunately, there exists no experimental measurements for this process with which to compare.

In Fig. 2, we present ejected-energy differential cross sec-

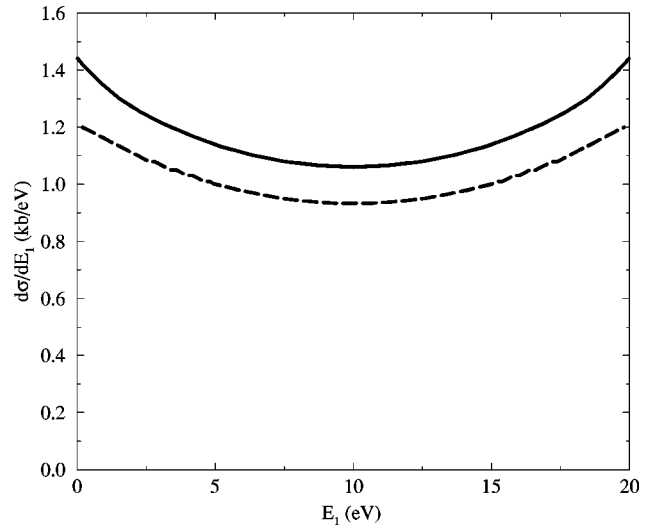

FIG. 2. Single energy differential cross section in kb/eV for beryllium at 20 eV excess photon energy. The solid line is the time-dependent close-coupling calculation and the dashed line is the convergent close-coupling calculation. (1.0 kb$=1.0\times10^{-21}$ cm^2.)

tions for Be at an excess photon energy of 20 eV, along with a convergent close-coupling calculation [17]. As in our previous work on helium [14], we retain the practice of multiplying the single differential cross sections by two, following the convention of the experiments on helium, which only measured cross sections from 0 to $E/2$. The cross sections are quite smooth for all values of E_1, the energy of one of the electrons, from 0–20 eV. The cross section has a deeper ''smile'' shape than the equivalent ejected-energy differential cross sections for He at the same excess photon energy [14], due to the lower double ionization threshold in beryllium (27.6 eV compared to 79 eV). Again, our calculations are in good agreement with the very recent convergent close-coupling calculations [25], with the difference between the two calculations being due to the small difference in the total cross section at this excess energy. There are no experimental results available with which to compare this process.

In our previous calculations of double photoionization of helium at 20 eV excess photon energy, it was sufficient to go up to $l=3$ in the expansions over the angular momentum pairs in Eqs. (6) and (9) to achieve well-converged triple differential cross sections. For the beryllium atom, the convergence is much more slow. In Fig. 3, we present triple differential cross sections when the angle of the first ejected $\theta_1=0$, at a coplanar geometry, and at 20 eV excess photon energy, for the case of equal energy sharing between the electrons ($E_1=E_2=10$ eV). We show cross sections which were calculated with (a) $l_0\leqslant2,l_1,l_2\leqslant3$, (b) $l_0\leqslant3,l_1,l_2\leqslant4$, (c) $l_0\leqslant4,l_1,l_2\leqslant5$, and (d) $l_0\leqslant5,l_1,l_2\leqslant6$, respectively, in Eqs. (6) and (9). It is clear that the triple differential cross section only completely converges for the final case, and that for the first two calculations, the triple differential cross sec-

TABLE I. Convergence of the total double photoionization cross section and the ejected-energy differential cross section at 20 eV excess photon energy, at equal energy sharing between the two electrons, for maximum values of l_0 and l_1, l_2 in Eqs. (6) and (9). (1.0 kb $= 1.0 \times 10^{-21}$ cm^2.)

l_0	l_1, l_2	σ (kb)	$\frac{d\sigma}{dE_1}(E/2)$ (kb/eV)
2	3	11.9	1.00
3	4	12.6	1.11
4	5	12.0	1.07
5	6	11.9	1.06

tion is quite different in shape and magnitude in comparison with the final result. Indeed, for (a) and (b), the triple differential cross section is quite unphysical, since it predicts a maximum in the cross section at $\theta_2 = 0$, which implies both electrons being ejected with equal energy along the same path, which is clearly incorrect.

This is in contrast to the convergence of the total double photoionization cross section, and the ejected-energy differential cross section, where the convergence is shown in Table I. Here, the cross sections do not change significantly with respect to the number of angular momenta in Eqs. (6) and (9). This implies that great care must be taken in the determination of triple differential cross sections, since the apparent convergence in total or single differential cross sections does not mean that triple differential cross sections are necessarily converged. The sensitivity of the shape of the triple differential cross sections to the number of angular momenta mean that convergence with respect to these parameters must be rigorously checked in all cases.

Satisfied that our triple differential cross sections are converged with respect to the angular momentum expansions, we turn our attention to comparisons with the only other theoretical calculations [25]. Again, no experimental measurements are available for this process. In Fig. 4, we present triple differential cross sections for beryllium as a function of θ_2, for various values of θ_1, as indicated, and for equal energy sharing $E_1 = E_2 = 10$ eV between the two ejected electrons. The solid lines are the current time-dependent close-coupling calculations and the dashed lines are the convergent close-coupling calculations of [25]. We can see that, in general, the agreement between the two nonperturbative theories is very good, with the exception of the small $|\theta_2|$ region when $\theta_1 = 0°$. Although the peaks heights of the calculations of the two theories are slightly different, the position and widths of the peaks are in excellent agreement. Qualitatively, the triple differential cross sections for beryllium at this excess energy are very similar to those obtained for helium. Apart from the peak heights, which are larger in beryllium due to the larger total double photoionization cross section, the shapes are almost identical in position and width. This implies that removal of the two $2s^2$ electrons in beryllium is very similar to the removal of the two $1s^2$ electrons in helium at this relatively low photon energy.

In Fig. 5, we present triple differential cross sections as a function of θ_2, for $\theta_1 = 0$, for three values of the first ejected electron energy E_1, as indicated. As expected, the cross section is virtually zero near $\theta_2 = 0$, since we do not expect the two electrons to be ejected in the same direction, even for very unequal energy sharing between the electrons. In comparison with the equivalent triple differential cross sections for helium, the shapes of the cross section are broadly the same, with the position of the peaks unchanged. However, it is interesting to note that for $E_1 = 3$ eV, the peaks present in the beryllium cross section at approximately $|\theta_2| = 100°$ are very much suppressed. It is unclear at this stage why this

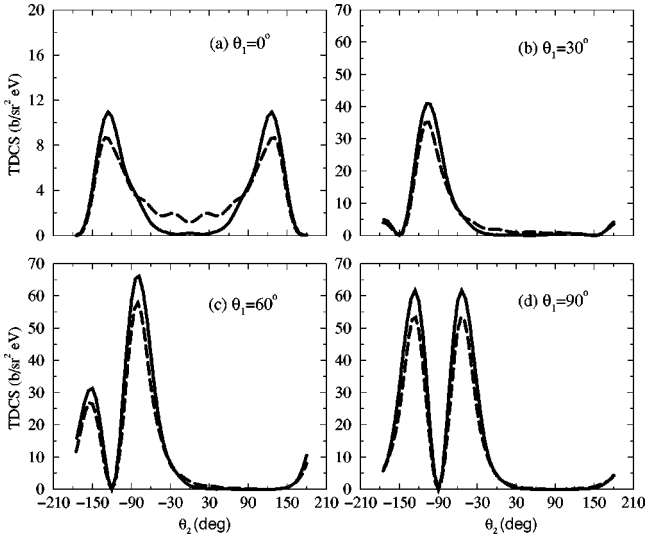

FIG. 4. Triple differential cross section in b/sr^2 eV for beryllium as a function of θ_2, the angle of the second ejected electron, for different fixed values of θ_1 as indicated and for equal energy sharing $E_1 = E_2 = 10$ eV between the two ejected electrons. The solid lines are the current time-dependent close-coupling calculations and the dashed lines are the convergent close-coupling calculations of [25]. (1.0 b $= 1.0 \times 10^{-24}$ cm^2.)

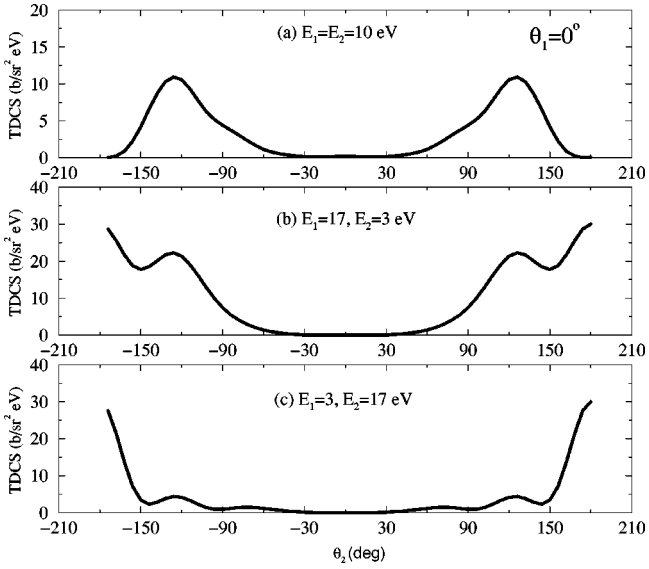

FIG. 5. Triple differential cross section in b/sr^2 eV for beryllium as a function of θ_2, the angle of the second ejected electron, for $\theta_1 = 0°$, for different energy sharing as indicated between the two ejected electrons. (1.0 b $= 1.0 \times 10^{-24}$ cm^2.)

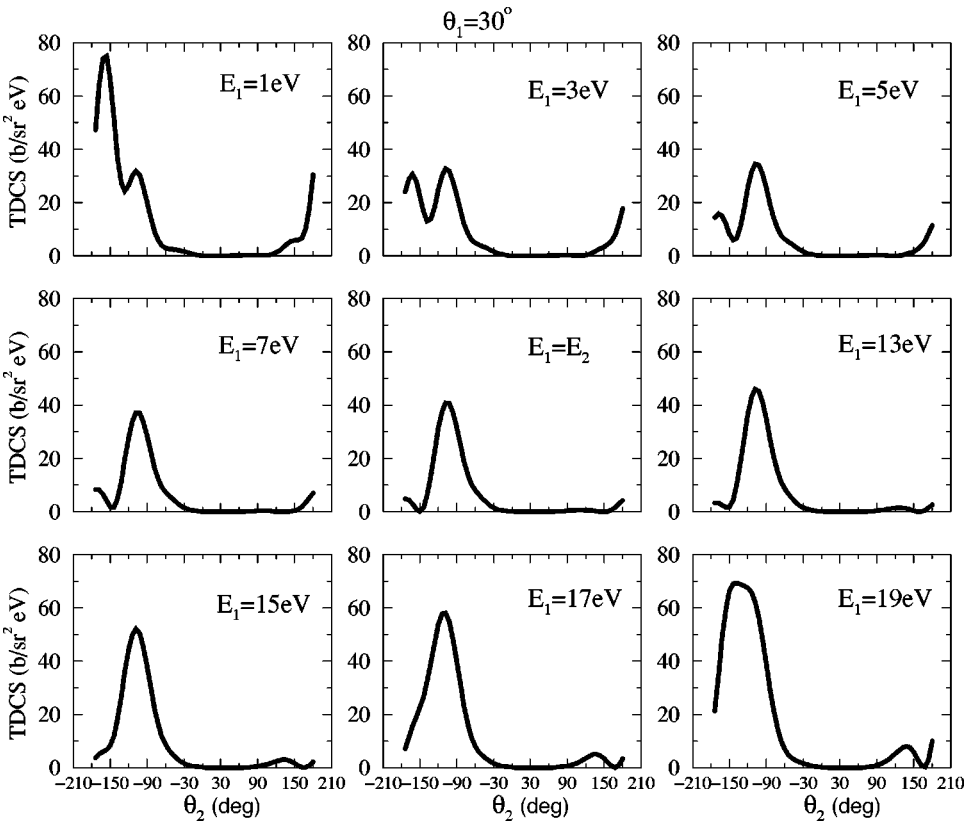

FIG. 6. Triple differential cross section in b/sr^2 eV for beryllium as a function of θ_2, the angle of the second ejected electron for $\theta_1 = 30°$ for a range of energy sharing as indicated between the two ejected electrons. (1.0 b $= 1.0 \times 10^{-24}$ cm^2.)

should be so, particularly as the peaks at $E_1 = 17$ eV are still evident.

To complete our comparison with triple differential cross sections for helium at 20 eV excess photon energy, we present in Fig. 6 cross sections for beryllium as a function of θ_2, with $\theta_1 = 30^o$, at a wide range of energy sharings between the two ejected electrons. The cross sections for beryllium show many similarities to the equivalent cross sections for helium, in the position and widths of the peaks, although the magnitude is generally higher than in helium. Again, at the cases of most unequal energy sharing, ($E_1 = 1$ eV, and $E_2 = 1$ eV) there are some differences in the shape of the cross sections as compared with helium.

IV. SUMMARY

In this paper, we have presented absolute calculations of the total integral, single differential and triple differential cross sections for the double photoionization of beryllium using a time-dependent close-coupling technique. We believe that this marks one of the first such absolute calculations of these processes for an alkaline-earth element. It is worth noting that once the time-dependent calculation has generated the complex momentum amplitudes, any conceivable angular differential cross section may be calculated in a straightforward manner for any possible combination of angular and/or energy sharings.

Our nonperturbative time-dependent calculations for total integral cross sections are considerably lower than previous perturbative calculations [15,16], but are in very good agreement with another current nonperturbative theoretical calculation [17]. This is all the more remarkable due to the completely different nature of the nonperturbative calculations, and the increased complexity of the beryllium target. We are aware of no experimental measurements of any total or differential cross sections for double ionization of beryllium with which to compare. As well as presenting ejected-energy single differential cross sections, we have made a detailed study of triple differential cross sections in beryllium, and compared our results with previous calculations of triple differential cross sections in helium [14]. We have found that convergence with respect to the number of angular momenta included in a calculation is critical in determining the correct triple differential cross section. It is apparent that without establishing convergence, completely unphysical triple differential cross sections may be obtained. Although experiments using beryllium are generally difficult, it is hoped that these calculations will stimulate more experimental work in measuring absolute differential cross sections of the alkaline-earth metals, continuing the pioneering work in recent years on helium.

ACKNOWLEDGMENTS

We would like to thank F. Robicheaux for useful discussions, and I. Bray for communicating his results before publication. This work was supported in part by the U.S. National Science Foundation, and the U.S. Department of Energy. Computational work was carried out at the National Energy Research Supercomputer Center in Oakland, CA.

[1] J. C. Levin, G. B. Armen, and I. A. Sellin, Phys. Rev. Lett. **76**, 1220 (1996).
[2] R. Dörner, T. Vogt, V. Mergel, H. Klemliche, S. Kravis, C. L. Cocke, J. Ullrich, M. Unverzagt, L. Speilberger, M. Damrau, O. Jagutski, I. Ali, B. Weaver, K. Ullmann, C. C. Hsu, M. Jung, E. P. Kanter, B. Sonntag, M. H. Prior, E. Rotenberg, J. Denlinger, T. Warwick, S. T. Manson, and H. Schmidt-Böcking, Phys. Rev. Lett. **76**, 2654 (1996).
[3] J. A. R. Samson, W. C. Stolte, Z. X. He, J. N. Cutler, Y. Lu, and R. J. Bartlett, Phys. Rev. A **57**, 1906 (1998).
[4] R. Dörner, H. Braüning, J. M. Feagin, V. Mergel, O. Jagutzki, L. Speilberger, T. Vogt, H. Khemliche, M. H. Prior, J. Ullrich, C. L. Cocke, and H. Schmidt-Böcking, Phys. Rev. A **57**, 1074 (1998).
[5] H. Braüning, R. Dörner, C. L. Cocke, M. H. Prior, B. Krässig, A. S. Kheifets, I. Bray, A. Braüning-Demian, K. Carnes, S. Dreuil, V. Mergel, P. Richard, J. Ullrich, and H. Schmidt-Böcking, J. Phys. B **31**, 5149 (1998).
[6] M. Achler, V. Mergel, L. Spielberger, R. Dörner, Y. Azuma, and H. Schmidt-Böcking, J. Phys. B **34**, 965 (2001).
[7] D. Proulx and R. Shakeshaft, Phys. Rev. A **48**, R875 (1993).
[8] M. Pont, R. Shakeshaft, F. Maulbetsch, and J. S. Briggs, Phys. Rev. A **53**, 3671 (1996).
[9] A. S. Kheifets and I. Bray, J. Phys. B **31**, L447 (1998).
[10] A. S. Kheifets and I. Bray, Phys. Rev. A **62**, 065402 (2000).
[11] L. Malegat, P. Selles, and A. K. Kazansky, Phys. Rev. A **60**, 3667 (1999).
[12] L. Malegat, P. Selles, and A. K. Kazansky, Phys. Rev. Lett. **85**, 4450 (2000).
[13] M. S. Pindzola and F. Robicheaux, Phys. Rev. A **57**, 318 (1998); **58**, 779 (1998).
[14] J. Colgan, M. S. Pindzola, and F. Robicheaux, J. Phys. B **34**, L457 (2001).
[15] P. Winkler, J. Phys. B **10**, L693 (1977).
[16] S. M. Varnavskikh, Opt. Spectrosc. **49**, 644 (1980).
[17] A. Kheifets and I. Bray, Phys. Rev. A (to be published).
[18] K. J. Ross, J. B. West, and H.-J. Beyer, J. Phys. B **30**, L735 (1997).
[19] K. J. Ross, J. B. West, H.-J. Beyer, and A. De Fanis, J. Phys. B **32**, 2927 (1999).
[20] H.-J. Beyer, J. B. West, K. J. Ross, and A. De Fanis, J. Phys. B **33**, L767 (2000).
[21] S. C. Ceraulo, R. M. Stehmann, and R. S. Berry, Phys. Rev. A **49**, 1730 (1994).
[22] A. K. Kazansky and V. N. Ostrovsky, J. Phys. B **30**, L835 (1997).
[23] See NIST's public website *http://physics.nist.gov/*.
[24] *Atomic Energy Levels I*, Natl. Bur. Stand. U.S. NSRDS No. 35, edited by C. E. Moore (U.S. GPO, Washington, D.C., 1971).
[25] A. Kheifets and I. Bray (private communication).